Optics and Photonics Journal, 2026, 16(3), 37-60
https://www.scirp.org/journal/opj
ISSN Online: 2160-889X
ISSN Print: 2160-8881

Low-Cost Scanning Beam Profiler Architectures for Near-Infrared Laser Characterization: Experimental Validation and Comparative Simulation

Haitian Liu, Christi Kay Madsen

Department of Electrical and Computer Engineering, Texas A&M University, College Station, USA
Email: cmadsen@tamu.edu, liuhaitian@tamu.edu

How to cite this paper: Liu, H.T. and Madsen, C. K. (2026) Low-Cost Scanning Beam Profiler Architectures for Near-Infrared Laser Characterization: Experimental Validation and Comparative Simulation. *Optics and Photonics Journal*, **16**, 37-60.
https://doi.org/10.4236/opj.2026.163003

Received: February 10, 2026
Accepted: March 28, 2026
Published: March 31, 2026

Copyright © 2026 by author(s) and Scientific Research Publishing Inc.
This work is licensed under the Creative Commons Attribution International License (CC BY 4.0).
http://creativecommons.org/licenses/by/4.0/
Open Access

Abstract

We present a low-cost beam profiling system based on a rotating photodiode detector for the characterization of near-infrared laser beams. Commercial beam profilers operating in this wavelength range are often costly and rely on specialized detector arrays with a limited wavelength range, while common silicon cameras are insensitive above 1.1 μm. The proposed system employs a single photodiode on a rotating arm, digitized by a microcontroller-based platform, enabling one-dimensional reconstruction of the beam intensity distribution at substantially reduced cost and complexity. Experimental validation at 1550 nm demonstrates approximately 10% agreement with a commercial Thorlabs scanning-slit beam profiler over the observed operating range, where the beam diameter spans at least three detector aperture widths. This agreement is comparable to the manufacturer-specified accuracy of commercial scanning-slit profilers, while the proposed system costs approximately one-twentieth as much. The wavelength coverage can also be extended from 800 to 2600 nm through detector substitution alone. Two alternative architectures are introduced through simulation: a single-mirror galvanometer for high-speed one-dimensional scanning, and a hybrid rotating-arm plus galvanometer system that combines two orthogonal one-dimensional scans to achieve full two-dimensional beam reconstruction.

Keywords

Beam Profiling, Near-Infrared Lasers, Rotating Photodiode, Laser Beam Characterization, Galvanometer Scanning

1. Introduction

Laser beam profiling is widely used for the characterization of beam size, spatial intensity distribution, and propagation properties in optical systems [1]. Accurate beam measurements are essential [2] [3] in applications such as fiber lasers [4], free-space optical communications [5], optical sensing [6], and material research and development (R&D) [7]. Common beam profiling techniques include camera-based imaging systems [8], knife-edge measurements [9], slit scanners [10], and scanning profiler methods [11] [12].

For near-infrared wavelengths around 1.55 μm, commercial beam profilers are often expensive because they require specialized detector technologies with extended infrared sensitivity. For example, InGaAs camera arrays are often expensive, typically costing $5k to $20k. Common silicon cameras stop at around 1.1 μm, which introduces the wavelength gap issue. As a result, low-cost alternatives are of interest for research laboratories and educational environments.

In this work, a low-cost beam profiling system based on a rotating detector is presented. A single photodetector is mechanically translated or rotated to sample the optical intensity distribution and reconstruct the beam profile. The photodiode measures the light intensity across the target plane, and the generated photocurrent is converted into a voltage signal using a transimpedance amplifier (TIA), whose gain is determined by the feedback resistor. The acquired analog signal is digitized by a microprocessor-based data acquisition system with an analog-to-digital converter (ADC), and the measured data are processed and analyzed in MATLAB. A systematic comparison between rotating-detector and galvo-scanning beam profilers operating in the near-infrared wavelength range is also presented, addressing a gap in the existing literature. In addition, a hybrid beam profiling architecture is proposed and discussed.

The paper first presents the geometric model and the detector noise model of the proposed system. Experimental validation is then carried out using a 1550 nm laser source. The measured beam profiles are compared with those obtained using a commercial beam profiler, and the close agreement between the two sets of results demonstrates the feasibility of the proposed approach for low-cost near-infrared beam characterization. Finally, simulations are conducted to compare the performance of three beam profiling architectures: the rotating detector, the single-mirror galvo scanner, and the proposed hybrid structure.

2. Theory Analysis

2.1. Geometric Model

Figure 1 shows the geometric model of the proposed scanning beam profiler for fiber to free space propagation. A single photodiode detector is mounted on a motorized rotary stage and rotated around the beam axis to acquire intensity measurements at multiple angular positions. The detector signal is recorded using a microcontroller-based data acquisition system. A transimpedance amplifier converts the photocurrent into voltage, and a fast-sampling analog-to-digital

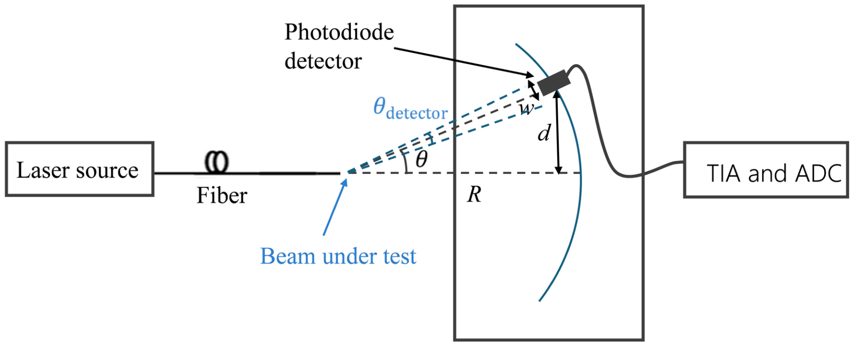

Figure 1. Schematic diagram of the beam profiler using the scanning photodiode method.

converter (ADC) enables real-time data acquisition.

The angle between the fiber end and the detector is represented as θ. Assuming the beam under test diverges slowly ($\theta \ll 1$), the small angle approximation gives

$$\theta \approx \tan\theta = \frac{d}{R}, \tag{1}$$

where d is the displacement in the target plane, and R is the length of the rotating arm.

From Equation (1), we can find that the translational displacement can be uniquely mapped to the corresponding angular position. A one-dimensional beam profiler measures the light intensity distribution along a line, which corresponds to the intensity distribution over a small angular range. If the rotating detector moves at a constant speed, the sampled data points on the target plane are uniformly distributed. The number of samples is defined as

$$N_{samples} = \frac{2\theta}{\Delta\theta}, \tag{2}$$

where $\Delta\theta$ is the motor step size and θ is half of the scanning range. It is related to the stepper motor mode. For example, if we utilize the Microstep (×16) mode of a stepper motor with a 1.8˚ standard step size, it gives us:

$$\Delta\theta = \frac{\text{Step angle}}{\text{gear ratio}} = \frac{1.8^\circ}{16} = 0.1125^\circ. \tag{3}$$

The angular resolution of this system is limited by both the motor step size $\Delta\theta$ and the detector angle $\theta_{detector}$. The detector spatially averages the incident intensity over its finite width $w_{detector}$. The detector angle is defined as

$$\theta_{detector} = \frac{w_{detector}}{R}. \tag{4}$$

The effective resolution θ_{eff} (worst case) is dominated by the larger value between the motor step size and the minimum resolution of the detector:

$$\theta_{eff} \equiv \max\{\Delta\theta, \theta_{detector}\}. \tag{5}$$

The spatial resolution in the translational target plane is

$$\Delta x = R \times \Delta\theta. \tag{6}$$

To consider the performance limit of the system, the minimum measurable beam diameter must be satisfied:

$$D_{beam_{min}} = N \times \Delta x , \tag{7}$$

where N is the number of data points collected across the profile. The spatial resolution can be chosen to be smaller or approximately equal to the detector width. Although the spatial resolution is limited by the detector aperture width $w_{detector}$ rather than the motor step size Δx, maintaining $\Delta x < w_{detector}/2$ provides two practical benefits: it satisfies the Nyquist sampling criterion for the aperture-filtered intensity distribution, enabling post-processing deconvolution to partially recover sub-aperture spatial information, and it improves beam centroid accuracy through Gaussian fitting. For our current system detailed below, Δx = 114 μm satisfies this criterion with respect to $w_{detector} = 300\ \mu\text{m}$.

The maximum measurable beam diameter should satisfy the small divergence angle ($\theta \ll 1$) condition; otherwise, the arc of the rotary detector trace cannot be considered as a plane. From Equation (1):

$$D_{beam_{max}} = 2d \ll 2R . \tag{8}$$

2.2. Detector Noise Model

To investigate the minimum measurable power, we must construct a noise detector model [13]. The power received at the detector aperture is:

$$P_{inc}(x,z) = \iint_{det} I(x,y,z)\,\mathrm{d}x\mathrm{d}y \approx I(x,y,z) \times A_{det} \approx I(x,z) \times w_{detector}^2 , \tag{9}$$

Assuming the detector is much smaller than the beam size so that light intensity is uniformly distributed inside the detector area. $P_{inc}(x,z)$ is optical power, and $I(x,z)$ is the light intensity measured by the detector aperture placed at position (x,z). x represents the transverse position from the center axis of the beam, and z represents the axial distance from the beam waist.

From the Gaussian beam model, the light intensity at the radial distance x and axial distance z is

$$I(x,z) = I_0 \left(\frac{w_0}{w(z)} \right)^2 \exp\left(\frac{-2x^2}{w(z)^2} \right), \tag{10}$$

where w_0 is the beam waist and I_0 is the intensity at the center of the beam at the waist:

$$I_0 = \frac{2P_0}{\pi w_0^2} . \tag{11}$$

$\boldsymbol{P_0}$ is the total power of the beam.

The beam waist at the axial position z is

$$w(z) = w_0 \sqrt{1 + \left(\frac{z}{z_R} \right)^2} , \tag{12}$$

where

$$z_R = \frac{\pi w_0^2 n}{\lambda} \tag{13}$$

is called the Rayleigh range, and n is the refractive index of the medium.

The signal photocurrent of the photodiode at the position (x,z) is:

$$I_{sig}(x,z) = R(\lambda)\times P_{inc}(x,z) = R(\lambda)\times I(x,z)\times w_{detector}^2, \tag{14}$$

where $R(\lambda)$ is the responsivity (A/W) under λ wavelength, and $P_{inc}(x,z)$ is the optical power on the detector aperture at the position (x,z).

In terms of systematic noise, the total noise comes from three sources:

1) The shot noise (dark)

$$I_{sd} = \sqrt{2qI_{dark}B} \tag{15}$$

q is the electron charge, B is the bandwidth, and I_{dark} is the dark current of the photodiode.

2) Thermal (Johnson) noise

$$I_j = \sqrt{\frac{4K_bT_n}{R_{sh}}B} \tag{16}$$

K_b is the Boltzmann constant, T_n is the temperature in Kelvin, and R_{sh} is the shunt resistance.

3) Amplifier noise I_{amp}, whose value is usually specified with the amplifier model.

The total diode current is contributed by the above three noise sources :

$$I_{noise} = \sqrt{I_{sd}^2 + I_j^2 + I_{amp}^2}. \tag{17}$$

The signal-to-noise ratio (SNR) measured at position (x,z) is defined as:

$$\mathrm{SNR}(x,z) = \frac{I_{sig}(x,z)}{I_{noise}} = \frac{R(\lambda)\times I(x,z)\times w_{detector}^2}{\sqrt{I_{sd}^2 + I_j^2 + I_{amp}^2}}$$

$$= \frac{R(\lambda)\times w_{detector}^2 \times \frac{2P_0}{\pi w_0^2} \times \frac{1}{1+\frac{z^2\lambda^2}{\pi^2 w_0^4 n^2}} \times \exp\left(\frac{-2x^2}{w_0^2\left(1+\frac{z^2\lambda^2}{\pi^2 w_0^4 n^2}\right)}\right)}{\sqrt{2qI_{dark}B + \frac{4K_bT_n}{R_{sh}}B + I_{amp}^2}}. \tag{18}$$

3. Experimental Validation

3.1. Experimental Setup

Table 1 lists the equipment we used to validate the proposed system. We conducted the gradient refractive index (GRIN) lens to free-space propagation experiment, which is the field of interest for many applications [14]. The light is coupled from a GRIN lens, which is mounted on top of a single-mode fiber end, to free space. A CW laser configured at 1550 nm serves as the light source, whose power level is set at 0.77mW. The InGaAs near-infrared photodiode (model

Table 1. Key components and specifications of the experiment.

Key components	Performance metrics	
	Key spec	Symbol and value
Pocket OTDR (FKEQU-094) 1550 nm laser	0.77 mW power	$P_0 = 0.77$ mW
Thorlabs PD box 366 GRIN lens	0.25-degree beam divergence	$w_0 = 0.176$ mm
2-axis positioner	for precise translation	
Marktech MTPD2601T-030 IR photodiode [15]	0.3 mm active area, 800–2600 nm, 0.8 A/W responsivity @1550 nm, 120 nA dark current, 3.4 kOhm shunt resistance	$w_{detector} = 0.3$ mm $R(1550\text{ nm}) = 0.8$ A/W $I_{dark} = 120$ nA $R_{sh} = 3.4$ kΩ
NEMA 17 stepper motor	Microstep mode, ±5˚ scan range	$\Delta\theta = 0.1125^\circ$ $\theta = 5^\circ$
Thorlabs BP109-IR Beam Profiler	For comparison, 700–1800 nm, 10 frames averaged.	
Plastic arm of the rotating detector	5.8-cm-long, 3D-printed	$R = 58$ mm
Transimpedance amplifier (TIA) and analog-to-digital converter (ADC)	Converting photocurrent to voltage with a gain equal to the feedback resistance	$R_{feed} = 330\ \Omega$ $I_{amp} = 2$ pA
Microprocessor-based data collection	with interface to Matlab for data analysis	

Marktech MTPD2601T-030) has an active area width of 0.3 mm and responsivity 0.8A/W@1550nm. The detector is fixed at a 5.8-cm long 3D-printed arm, which is driven by a NEMA 17 motor. The microstepping resolution was verified experimentally by commanding 80 steps and measuring the resulting rotation angle of approximately 9˚. The transimpedance amplifier (TIA) gain is 330 V/A, set by a 330 Ω feedback resistor. The ADC resolution (with unity gain setting) is 125 µV per LSB. The data acquisition is done through an ESP32 microprocessor with interface to Matlab for data analysis.

To compare the performance of our low-cost beam profiler with the commercial one, a Thorlabs BP209-IR knife-edge beam profiler is used as a reference.

3.2. Experimental Results

Figure 2 presents the measured beam profiles of the GRIN lens at propagation distances of 5 cm, 10 cm, 15 cm, and 20 cm. The upper plots show the raw measurement data acquired using the proposed rotating-detector system, while the lower plots illustrate the corresponding Gaussian fitting results. To evaluate the performance of the proposed system, the measured beam widths are compared with those obtained using a commercial Thorlabs beam profiler and with theoretical predictions based on Gaussian beam propagation. The measured beam profiles are fitted using the Gaussian intensity distribution.

$$I(x) = I_0 \exp\left[-2\left(\frac{x - x_0}{w}\right)^2\right], \tag{19}$$

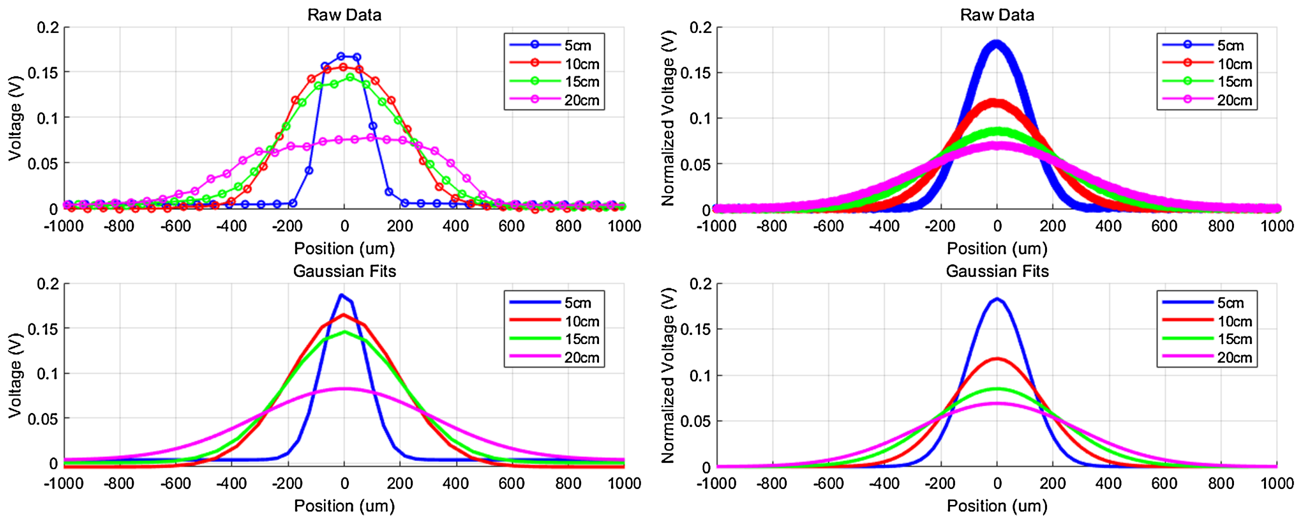

Figure 2. Plot of detected voltage vs. translational position at different longitudinal distances. Raw beam profile of the proposed low-cost beam profiler (top left); raw beam profile of the commercial beam profiler (top right); Gaussian fit of the low-cost beam profile (bottom left); Gaussian fit of the commercial beam profiler (bottom right).

where w is the $1/e^2$ intensity radius. Throughout this work, the reported beam width is defined as the Gaussian $1/e^2$ intensity diameter, $2w$. This definition is applied consistently to the beam widths obtained from the proposed beam profiler, the commercial Thorlabs beam profiler, and the theoretical Gaussian-beam calculations. Accordingly, all reported beam-width values represent the $1/e^2$ intensity diameter $2w$, rather than the full width at half maximum (FWHM) or the ISO 11146 second-moment beam diameter.

As expected, the measured beam width increases monotonically with propagation distance due to free-space diffraction after the GRIN lens. The experimental measurements obtained by the proposed profiler exhibit the same increasing trend, confirming that the system correctly captures the beam evolution during propagation.

Another noticeable feature is that the peak normalized voltage decreases as the propagation distance increases. This behavior is consistent with the energy conservation of the optical beam. Since the total optical power remains approximately constant, the beam energy is distributed over a larger cross-sectional area as the beam diverges. Consequently, the irradiance at the beam center decreases, resulting in a lower detector output voltage while the beam profile becomes broader.

The Gaussian fitting curves shown in Figure 2 demonstrate that the measured profiles closely follow the expected Gaussian distribution. The fitting process effectively suppresses the noise. The excellent agreement between the measured data and the fitted curves also verifies the good performance of the proposed rotating-detector scanning approach.

To evaluate scan-to-scan repeatability, two independent beam-profile measurements were performed at each propagation distance. Representative repeated measurements at 5 cm and 15 cm are shown in Figure 3. The two independent scans exhibit consistent beam-profile shapes and similar Gaussian fitting results, indicating good scan-to-scan repeatability of the proposed rotating-detector system. The repeatability is quantitatively characterized by the mean and standard deviation of the extracted beam diameters from the two independent measurements, as summarized in Table 2.

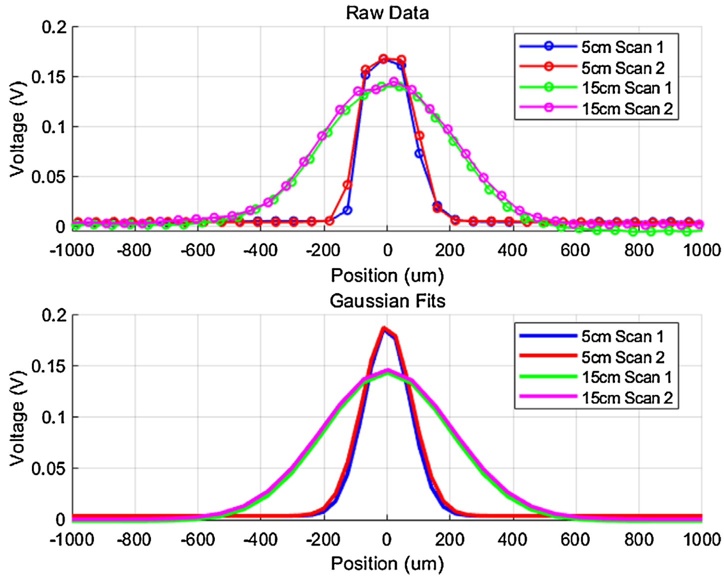

Figure 3. Representative repeated beam-profile measurements obtained from two independent scans at propagation distances of 5 cm and 15 cm.

Table 2. Quantitative comparison of the achieved beam width among the commercial Thorlabs beam profiler, the proposed rotating-detector beam profiler, and the theoretical calculation from Gaussian beam theory.

Measurement method and error analysis	Propagation distance			
	5 cm	10 cm	15 cm	20 cm
Thorlabs beam profiler	431 μm	646 μm	898 μm	1132 μm
Proposed beam profiler	302.1 ± 18.7 μm	743.9 ± 29.6 μm	815.1 ± 14.8 μm	1234.4 ± 22.5 μm
Theoretical calculation	450 μm	662 μm	912 μm	1175 μm
Error between the proposed and the commercial profiler	29.9%	15.1%	9.2%	9.0%
Error between the proposed profiler and the calculation	32.9%	12.4%	10.6%	5.1%

Table 2 compares the beam widths measured by the proposed system with those obtained using the commercial Thorlabs beam profiler and the theoretical Gaussian-beam calculations. Two independent measurements were performed at each propagation distance, and the beam widths obtained from the proposed system are reported as mean ± standard deviation to characterize the scan-to-scan repeatability. The proposed system measured beam diameters of 302.1 ± 18.7 μm, 743.9 ± 29.6 μm, 815.1 ± 14.8 μm, and 1234.4 ± 22.5 μm at propagation distances of 5 cm, 10 cm, 15 cm, and 20 cm, respectively. Compared with the commercial Thorlabs beam profiler, the corresponding relative errors based on the mean beam widths are 29.9%, 15.1%, 9.2%, and 9.0%, respectively. Relative to the theoretical Gaussian-beam calculations, the corresponding errors are 32.9%, 12.4%, 10.6%, and 5.1%, respectively.

The results indicate that approximately 10% agreement with the commercial Thorlabs beam profiler is observed for the larger beam diameters investigated in this study. In the present experiments, the beam diameters corresponding to approximately 10% agreement range from approximately 815 to 1234 μm, corresponding to approximately 2.7 to 4.1 detector aperture widths for the 300 μm detector used in this work. The standard deviations obtained from the two independent scans quantify the scan-to-scan variation, while the systematic differences between the mean measured values and the commercial reference are primarily associated with finite detector aperture and spatial sampling effects.

The agreement between the proposed system and the commercial reference improves as the propagation distance increases. At the shortest propagation distance of 5 cm, the beam diameter is relatively small and approaches the spatial sampling limit of the proposed profiler. Under these conditions, the finite detector aperture, discrete scanning step size, and positioning errors have a greater influence on the extracted beam width, resulting in larger deviations from both the commercial reference and theoretical prediction. As the beam propagates further, its diameter becomes larger relative to the detector aperture, increasing the number of spatial samples across the beam profile and reducing the influence of aperture averaging and spatial sampling limitations. Consequently, the measured beam widths show improved agreement with the theoretical Gaussian-beam calculations, with the smallest deviation of 5.1% observed at 20 cm.

Overall, the experimental results demonstrate that the proposed low-cost beam profiler can reliably characterize the evolution of Gaussian beam profiles over the experimentally investigated propagation range. The scan-to-scan repeatability measurements indicate consistent performance between independent measurements, while the comparison with the commercial Thorlabs beam profiler and theoretical Gaussian-beam calculations demonstrates improved agreement for larger beam diameters. Although the measurement deviation increases for relatively small beam diameters due to finite-aperture and spatial-sampling effects, the results confirm the feasibility of the proposed system for low-cost laser beam characterization.

3.3. Error Analysis

The discrepancies between the proposed profiler and the commercial beam profiler may originate from finite detector aperture, detector responsivity variation, motor positioning uncertainty, alignment error, and the noise introduced by the photodiode detector stated from Equations (15)-(17).

3.3.1. Detector Aperture Error

From Table 1 and Equations (1)-(8), we can specify some key performance metrics of the prototype system, which are listed in Table 3.

Table 3. Key performance metrics of the prototype system.

Key performance metrics	Symbol	Value
Stepper motor step size	$\Delta\theta$	0.1125˚
Detector angle	$\theta_{detector}$	0.296˚
Angular resolution	θ_{eff}	0.296˚
Spatial resolution	Δx	114 µm
minimum measurable beam diameter	$D_{beam_{min}}$	900 µm
maximum measurable beam diameter	$D_{beam_{max}}$	11.6 mm

Table 3 summarizes the fundamental performance parameters of the proposed beam profiler. The stepper motor provides a theoretical angular step size of 0.1125˚, whereas the detector subtends an angular width of 0.296˚. The detector's angular width is approximately 2.6 times larger than the motor step size.

The finite detector aperture introduces a systematic measurement error because the detector does not measure the optical intensity at a single point. Instead, the detector output corresponds to the average optical power incident over its active area. This averaging effect smooths the measured intensity distribution, causing the beam edges to become less steep and slightly broadening the reconstructed beam profile.

Based on the experimental results presented in Table 2, approximately 10% agreement with the commercial Thorlabs beam profiler is observed when the beam diameter exceeds approximately three detector aperture widths. For the 300 µm detector used in this work, this corresponds to a practical minimum measurable beam diameter of approximately 900 µm. This is consistent with the requirement for several independent spatial samples to support reliable Gaussian fitting [10], and reflects the combined influence of aperture averaging, discrete sampling, and mechanical positioning errors observed experimentally.

The influence of detector aperture becomes particularly significant when the beam diameter approaches the spatial resolution of the system. Under this condition, only a limited number of independent samples are available across the beam, and the convolution effect of the detector aperture causes the measured profile to deviate from the ideal Gaussian distribution. As the beam diameter increases, the detector occupies a much smaller fraction of the beam cross-section, reducing the averaging effect and allowing the reconstructed profile to more closely approximate the actual beam intensity distribution. This behavior is consistent with the experimental results presented in Table 2, where the beam-width error decreases as the beam diameter increases.

3.3.2. Mechanical Error

Besides the finite detector aperture, the measurement accuracy is also affected by the mechanical characteristics of the rotating scanning system. The beam profile is reconstructed from discrete angular samples generated by the stepper motor; therefore, any positioning error directly translates into spatial measurement uncertainty.

The first source of mechanical error is the stepper motor positioning accuracy. Although the theoretical step size is 0.1125˚, manufacturing tolerance, microstepping nonlinearity, and accumulated positioning errors introduce a small deviation in the actual rotation angle. The measured beam profile may be slightly shifted or broadened compared with the true optical intensity distribution.

If the motor step uncertainty is ±10% of one step, and the step size is 0.1125˚, then the angular uncertainty is ±0.01125˚, translating to a spatial uncertainty of 11.4 μm. At a 5 cm propagation distance, where the beam is 315 μm wide, this 11.4 μm uncertainty represents 3.6% of the beam width—a non-trivial contributor.

Mechanical vibration is another contributor to measurement uncertainty. During motor acceleration and deceleration, vibration of the rotating arm causes small fluctuations in the detector position. Although the motor is driven at a relatively low speed to minimize vibration, residual oscillations may still affect the measured detector output, particularly near the beam edge where the optical intensity gradient is large.

Furthermore, alignment errors between the laser beam axis and the rotational center of the scanning mechanism introduce systematic measurement offsets. If the optical axis does not perfectly coincidece with the detector rotation center, the reconstructed beam profile becomes asymmetric, leading to errors in the estimated beam center and beam width after Gaussian fitting.

Overall, the mechanical errors become more significant when measuring small beam diameters because the positioning uncertainty represents a larger fraction of the beam size. As the beam propagates and expands, the relative influence of these errors decreases, which is consistent with the experimental observation that the beam-width error reduces from approximately 32.9% at 5 cm to 5.1% at 20 cm.

3.3.3. Electronic Noise

Besides the detector aperture and mechanical errors, the measurement accuracy is also limited by electronic noise in the photodetection circuit. As derived in Equations (15)-(18), the total current noise consists of shot noise, thermal (Johnson) noise, and amplifier noise.

The photodiode signal was acquired using an ADS1015 ADC operated at its default conversion rate of approximately 1600 samples/s. In the scanning procedure, each measurement point consisted of one motor microstep followed by ADC acquisition, display updating, and serial data transmission. Therefore, the effective system-level acquisition bandwidth was substantially lower than the ADC conversion rate. Based on the estimated per-position acquisition cycle of approximately 10 ms, an effective acquisition bandwidth on the order of 100 Hz was used for the noise and SNR analysis. This bandwidth estimate was used to convert the calculated noise spectral densities into RMS noise values for evaluating the system SNR and dynamic range.

The shot noise is 1.96 pA, the Johnson noise is 22pA, and the amplifier noise is 2 pA. The total noise is 22.25 pA. Unlike the noise current, which is approximately constant for a given detector and amplifier configuration, the photocurrent is proportional to the optical intensity incident on the detector. Consequently, the signal-to-noise ratio varies across the beam profile according to Equation (18).

Figure 4 presents the theoretical SNR distribution calculated from Equation (18) for propagation distances of 5 cm, 10 cm, 15 cm, and 20 cm. Since the total electronic noise is assumed to remain constant under fixed detector and amplifier conditions, the spatial variation of the SNR is determined primarily by the optical intensity distribution.

The theoretical dynamic range (DR) of the proposed system is approximately 70 dB within one beam radius w and increases to approximately 277 dB within two beam radii. This analysis explains why the measurement of low-intensity beam tails beyond twice the beam radius becomes challenging without implementing gain switching or additional signal amplification.

Experimentally, the measured noise floor is approximately 1 mV, while the typical signal level is above 300 mV. This corresponds to a signal-to-noise ratio (SNR) greater than 300 and an experimental dynamic range of approximately 49.5 dB, which is lower than the theoretical prediction. The discrepancy is primarily attributed to the limited resolution of the ADC, which provides a voltage resolution of 125 μV per least significant bit (LSB) and introduces a quantization limit to the minimum detectable signal level.

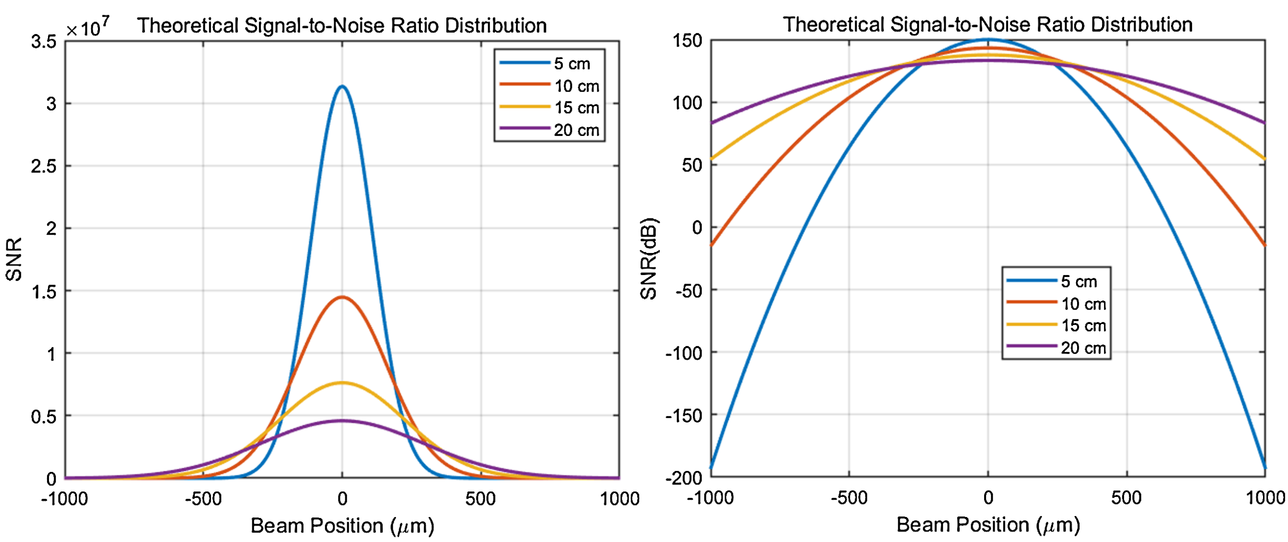

Figure 4. Theoretical signal-to-noise ratio of the proposed system in the (left) decimal scale and (right) logarithmic scale.

4. Simulation and Architecture Comparison

Beyond the proposed rotating-detector system, several alternative beam profiling architectures have been widely investigated, including the single-mirror galvanometer scanner, the hybrid rotating-arm plus single-mirror galvanometer system, and the dual-mirror galvanometer scanner [16] [17]. Their operating principles and performance characteristics are analyzed in this chapter to evaluate the advantages and limitations of each architecture and to highlight the motivation for the proposed system.

4.1. Single-Mirror Galvo

Figure 5(a) illustrates the configuration of a single-mirror galvanometer beam profiler. Unlike the proposed rotating-detector architecture, the photodiode detector remains stationary at the image plane, which is located at a distance d from the galvanometer mirror. The mirror rotates with discrete angular steps of $\Delta\theta$, causing the reflected laser beam to scan across the image plane. The corresponding spatial resolution is determined by Equation (6), where the scanning radius R is equal to d.

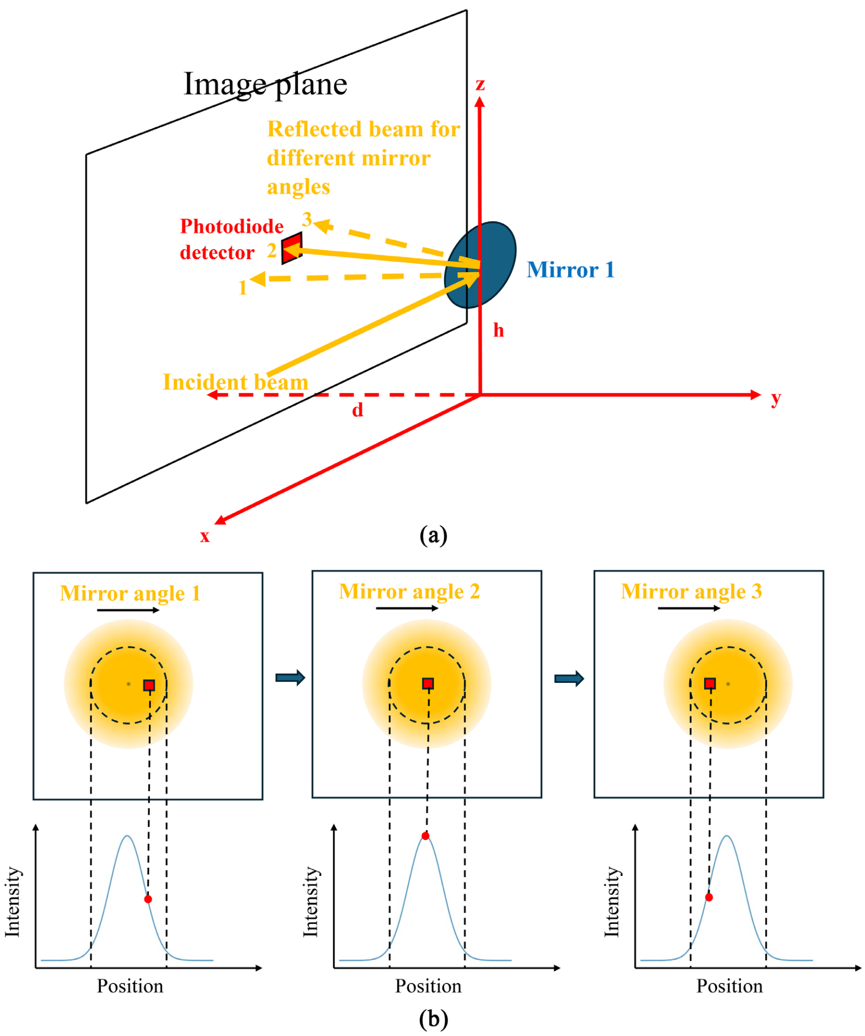

Figure 5. (a) Schematic diagram of the single-mirror galvo system. (b) Illustration of the working principle of the system.

Figure 5(b) illustrates the scanning principle. A photodiode with an active area significantly smaller than the beam diameter is fixed at the center of the image plane. The laser beam is assumed to be substantially larger than the detector aperture. As the scanning mirror continuously changes its angular position, the laser spot sweeps across the detector, allowing sequential sampling of the beam intensity along a single horizontal line. By combining all sampled intensity values with their corresponding spatial positions, a one-dimensional beam profile can be reconstructed.

Figure 6 presents the simulation results for a single-mirror galvanometer beam profiler with a typical mechanical angular resolution of 0.5 mrad and a mirror-to-image-plane distance of 5.8 cm. The galvanometer is assumed to scan over an angular range of ± 0.5˚, corresponding to a transverse scanning range of approximately ± 506 μm at the image plane. Considering the twofold angular deflection of the reflected beam, the corresponding optical angular sampling interval is 1

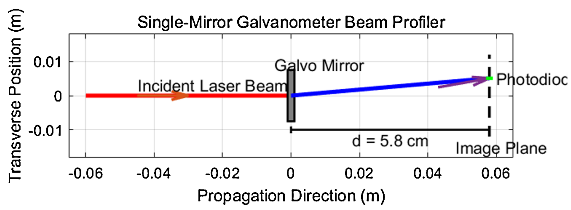

(a)

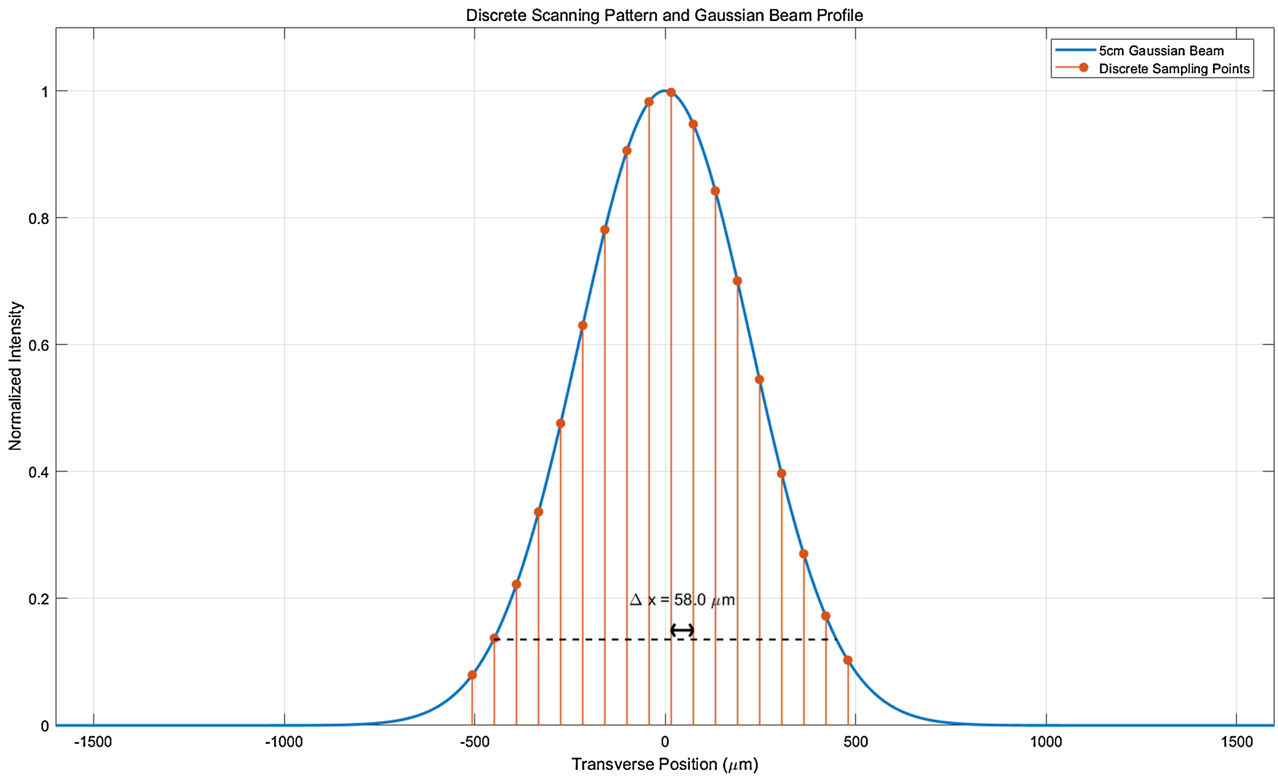

(b)

Figure 6. (a) Simulation diagram of the single-mirror galvanometer beam profiler. (b) Gaussian beam profile and corresponding discrete sampling points at a propagation distance of 5 cm with a ± 0.5˚ angular scanning range.

mrad, resulting in a spatial sampling interval of approximately 58 μm at the image plane. Figure 6(b) compares the Gaussian beam profile at a propagation distance of 5 cm with the discrete sampling points obtained from the simulated scanning process. Under the selected scanning range and sampling interval, approximately 16 sampling points are located within the beam profile, demonstrating the spatial sampling characteristics of the single-mirror galvanometer architecture.

At longer propagation distances, such as 10 cm, 15 cm, and 20 cm, the spatial sampling resolution remains unchanged because it is determined by the galvanometer angular resolution and the mirror-to-image-plane distance. Meanwhile, the Gaussian beam expands with propagation distance, resulting in more sampling points across the beam profile. Therefore, more than 16 data points can be obtained across the beam diameter, providing denser spatial sampling and potentially improving the accuracy of beam-profile reconstruction.

Compared with a mechanically rotating detector, the single-mirror galvanometer offers substantially higher scanning speed because only a lightweight mirror is actuated, enabling scanning frequencies to be increased from several hertz to several hundred hertz. Furthermore, modern galvo mirror drivers can achieve smaller angular resolutions, corresponding to better spatial resolutions compared to stepper-motor-driven systems. These characteristics make the single-mirror architecture particularly suitable for high-speed one-dimensional beam measurements.

However, the single-mirror configuration is inherently limited to one-dimensional scanning. Only the beam profile along the scanning direction can be directly measured, while the orthogonal beam dimension remains unknown. Consequently, this architecture cannot uniquely determine the full two-dimensional beam distribution. This limitation motivates the hybrid architecture discussed in the following section, which combines the high-speed scanning capability of a galvanometer with the angular diversity provided by a rotating detector arm.

4.2. Hybrid Architecture: Rotating Arm + Single-Mirror Galvo

Figure 7(a) illustrates the schematic diagram of the hybrid beam profiler, which

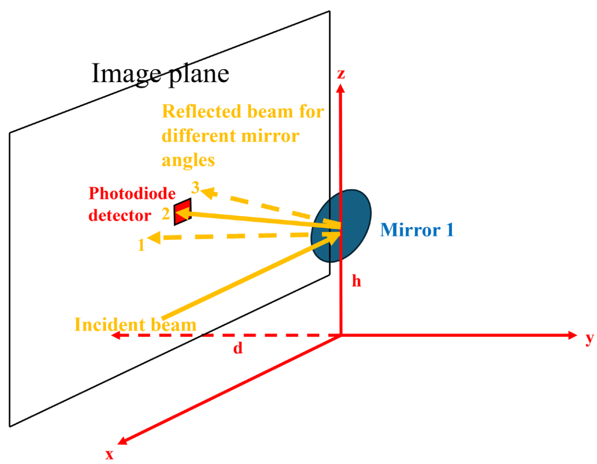

(a)

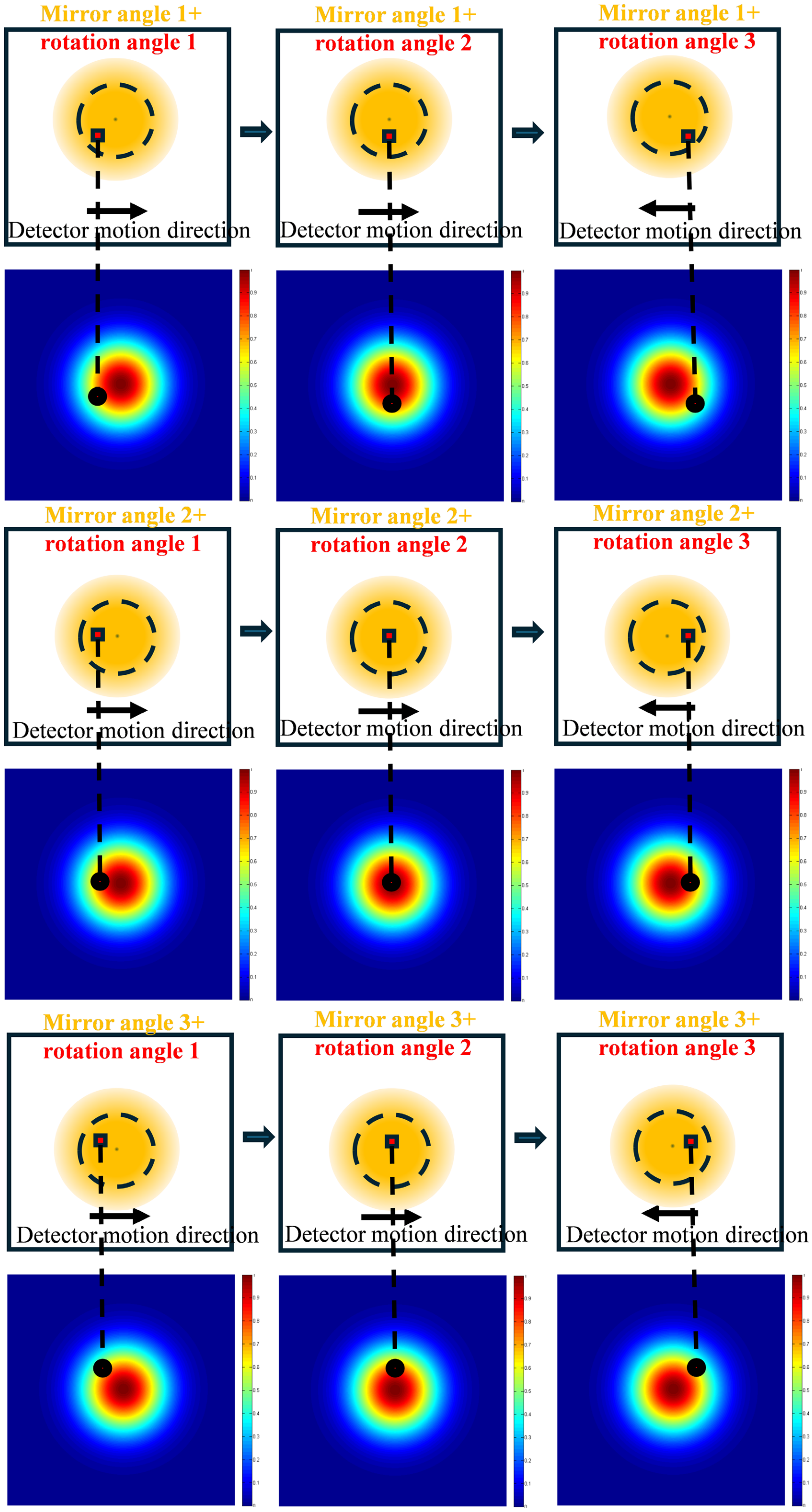

(b)

Figure 7. (a) Schematic diagram of the hybrid architecture consisting of a rotating arm and a single mirror. (b) Illustration of the working principle of the system.

combines a rotating arm with a single-axis scanning mirror. Like the proposed rotating detector system, the rotating arm is driven by a stepper motor to perform scanning along one axis (e.g., the horizontal direction). Meanwhile, the galvo mirror provides beam deflection in the orthogonal direction (e.g., the vertical direction). During operation, the mirror is first positioned at a fixed vertical angle, after which the rotating arm performs a complete scan across the horizontal axis. Once the horizontal scan is completed, the mirror steps to the next vertical position, and the process is repeated. By combining multiple one-dimensional scans acquired at different mirror positions, the two-dimensional beam intensity distribution can be reconstructed, as illustrated in Figure 7(b).

Figure 8 presents the simulation results of the proposed hybrid scanning system at a propagation distance of 5 cm, using the same beam parameters as those in Figure 6. The x axis represents the scanning direction of the rotating arm, which is driven by a stepper motor with an angular step size of $\Delta\theta = 0.1125^{\circ}$, while the y axis represents the scanning direction of the galvanometer mirror, with a

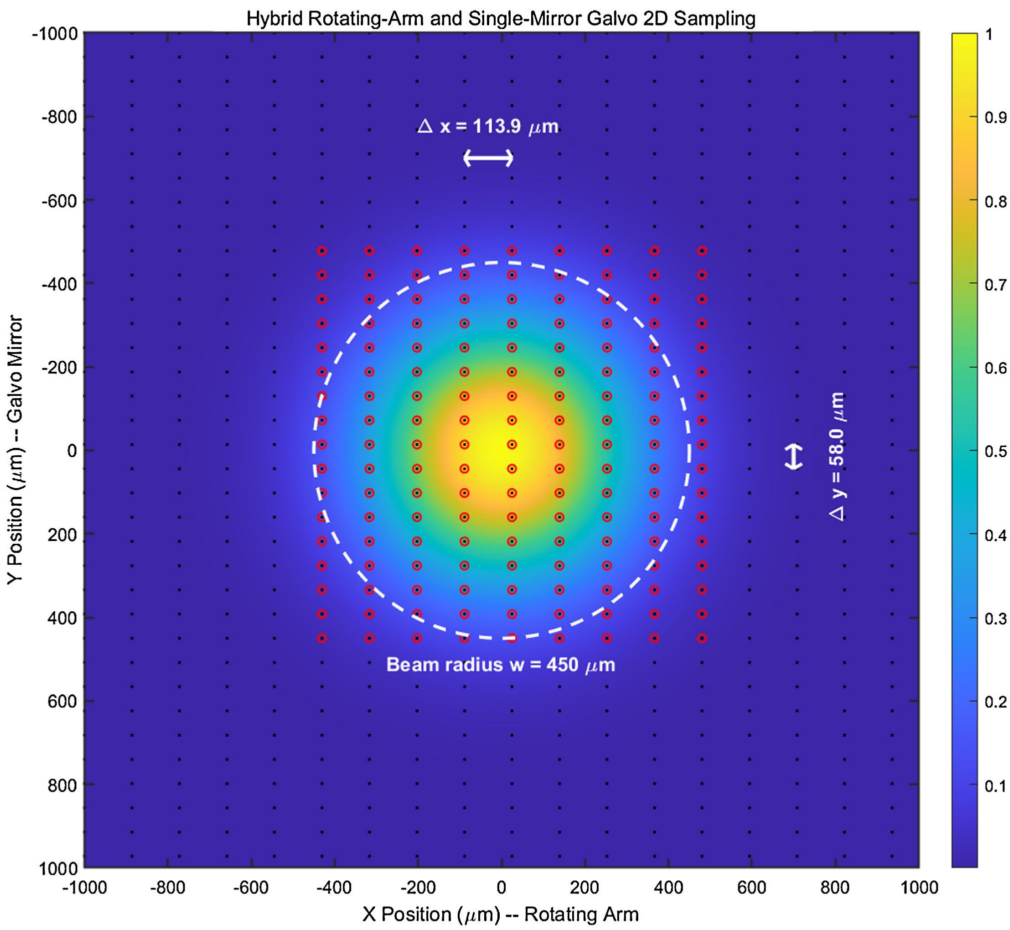

Figure 8. Simulation results of the proposed hybrid scanning system at a propagation distance of 5 cm, illustrating the Gaussian beam profile and a two-dimensional discrete sampling pattern with different spatial sampling intervals along the rotating-arm and galvanometer-mirror directions. The white dashed circle represents the beam radius of 450 μm. The red highlighted dots represent the sampling points within the ± 0.5˚ angular scanning range of the galvanometer mirror.

mechanical angular resolution of 0.5 mrad. Because the two scanning axes employ different angular resolutions and scanning mechanisms, the resulting spatial sampling intervals are different. The spatial sampling interval is approximately 113.9 μm in the x direction and 58 μm in the y direction. Within the beam profile, approximately 16 sampling points are obtained along the y direction, which is comparable to the sampling density of the single-mirror galvanometer system shown in Figure 6(b). In the x direction, approximately 8 sampling points are obtained across the beam profile. These results demonstrate that the proposed hybrid architecture provides anisotropic spatial sampling, with a higher sampling density along the galvanometer-mirror direction than along the rotating-arm direction.

Compared with a purely mechanical scanning system, the hybrid architecture significantly reduces the mechanical travel required in one dimension, enabling faster acquisition while maintaining a relatively simple system configuration. However, this approach introduces a potential limitation in spatial sampling. Since the horizontal and vertical directions are generated by two different scanning mechanisms, the achievable spatial resolutions along the two axes are generally different. The galvo scanning direction has the same spatial resolution as the single-mirror system, whereas the rotational scanning direction has the same resolution as the rotating-detector system. As a result, the reconstructed beam profile may exhibit anisotropic sampling, leading to rectangular rather than square pixels in the raster image.

To obtain a uniform two-dimensional raster scan, the effective spatial step sizes produced by the rotating arm and the galvo mirror should be closely matched. This requires careful calibration of the mirror angular increment relative to the motor step size so that adjacent sampling points have approximately equal spacing in both directions. If the two step sizes differ significantly, the reconstructed beam profile will suffer from unequal sampling density, potentially reducing measurement accuracy and introducing interpolation errors during image reconstruction. Therefore, the hybrid architecture offers a compromise between scanning speed and system complexity, but its performance relies on proper synchronization and matching of the two orthogonal scanning resolutions.

4.3. Two-Mirror Galvo

The final architecture is the two-mirror galvo beam profiler, as illustrated in Figure 9. In this configuration, two orthogonally mounted scanning mirrors are employed to achieve beam deflection in the horizontal and vertical directions. The two mirrors are separated by a distance h, with the second mirror located at a distance d from the image plane. By independently controlling the angular positions of the two mirrors, a two-dimensional raster scan of the incident beam can be achieved while keeping the photodetector stationary.

The spatial resolution along the horizontal direction is determined by the beam displacement generated by the second scanning mirror and can be expressed as

$$\Delta x = d * \tan\left(2\Delta\theta\right) \approx 2d\Delta\theta . \quad (20)$$

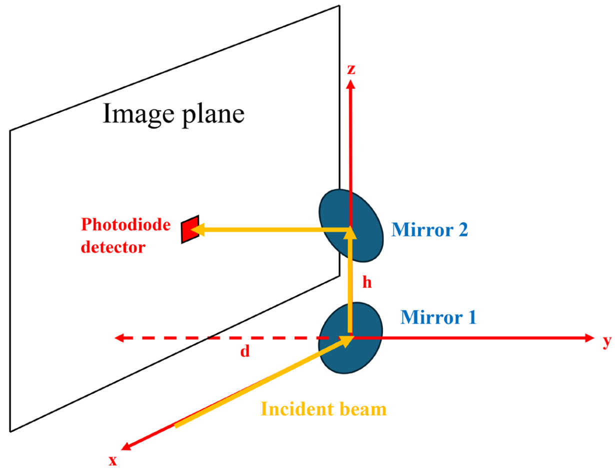

Figure 9. Schematic diagram of the two-mirror galvo system.

Similarly, the vertical resolution is given by

$$\Delta y = 2(h + d)\Delta\theta, \quad (21)$$

where $\Delta\theta$ denotes the angular resolution of the scanning mirrors. These equations indicate that the spatial resolution of the proposed system is primarily determined by the mirror angular resolution $\Delta\theta$, the mirror separation h, and the optical propagation distance d. For $\Delta\theta = 0.5$ mrad, $h = 20$ mm, and $d = 200$ mm, the theoretical spatial resolution is approximately 220 μm. In addition, the finite separation between the two mirrors introduces a lateral beam displacement given by

$$\Delta y_1 = h\sin(\theta_1). \quad (22)$$

For the present system, this displacement is approximately 1.74 mm at a scanning angle of $\theta_1 = \pm 5^\circ$, representing the primary geometric artifact that should be considered when high-accuracy beam profile reconstruction is required.

Compared with the rotating-detector architecture, the two-mirror galvo configuration provides true two-dimensional beam mapping without requiring mechanical translation of the detector, resulting in faster acquisition speed and improved measurement repeatability. However, the overall system performance depends strongly on the angular accuracy, synchronization, and stability of the scanning mirrors.

Table 4 summarizes the comparison between different beam profiling approaches. The proposed system achieves comparable beam characterization performance at approximately one order of magnitude lower cost than commercial beam profilers, while introducing trade-offs in terms of working wavelength, scanning speed, spatial resolution, and sensitivity to mechanical tolerances.

5. Discussion

The proposed rotating-detector beam profiler demonstrates that accurate near-infrared beam characterization can be achieved using inexpensive and readily available components. Experimental validation shows that the measured beam

Table 4. Comparison among different beam profiling systems.

Performance metrics	System			
	Proposed beam profiler	Single-mirror[a]	Hybrid architecture	Thorlabs beam profiler
Achitecture	Photodiode + motor-driven rotating arm	Photodiode + single mirror	Photodiode + motor-driven rotating arm + single mirror	Commercial camera-based system
Spatial resolution	~100 µm	~50 µm	Galvo axis: ~50 µm Rotation axis: ~100 µm	~10 µm
Cost	~$200 - 500	~$200 - 500	~$300 - 600	~$5000 - 8000
Working wavelength	Near-infrared, 800 - 2600 nm	mirror-limited, 1280 - 1600 nm	1280 - 1600 nm	700 - 1800 nm
Data acquisition time	~10 s seconds	Several seconds	~half a minute	Real time
Geometry	1D profiling	1D profiling	2D profiling	2D profiling

[a]The performance depends on the mirror specifications. The table values are based on the Thorlabs BB03-E04 fused silica dielectric mirror.

widths agree well with both theoretical Gaussian beam propagation and measurements obtained using a commercial beam profiler. The measurement error decreases as the beam diameter increases, indicating that the proposed system is particularly suitable for moderate and large beam sizes, where the influence of detector aperture and spatial sampling becomes less significant.

The experimental results indicate that approximately 10% agreement with the commercial Thorlabs beam profiler is observed over the demonstrated operating range when the beam diameter approaches or exceeds approximately three detector aperture widths. This observation is consistent with the general requirement that several independent spatial samples span the beam profile for reliable Gaussian width extraction. For smaller beam diameters, the measurement error increases as the number of detector aperture widths spanning the beam profile decreases. This behavior is attributed primarily to the finite-aperture averaging effect, which reduces the spatial resolution of the measured profile and contributes to the tendency toward underestimation of the beam width observed at shorter propagation distances.

The observed approximately 10% agreement with the commercial reference is comparable in magnitude to the manufacturer-specified beam-diameter accuracy of the Thorlabs BP209-IR scanning-slit profiler, which specifies errors of less than 10% for beam diameters measured using its maximum 9 mm aperture under optimal conditions (BP209-VIS(/M); BP209IR1(/M): Beam diameter error <10% at Ø9 mm). Notably, the Thorlabs BP209-IR2, a commercial instrument covering a similar NIR wavelength range, specifies beam-diameter errors of less than 20% under its optimal beam-size conditions (BP209-IR2(/M): Beam diameter error < 20% at Ø9 mm for beam divergence < 5˚) ([18], p. 145). These comparisons suggest that the proposed architecture can provide competitive beam-width measurement performance in the NIR wavelength range while substantially reducing system cost.

Compared with commercial camera-based beam profilers, the proposed system significantly reduces hardware cost by replacing expensive InGaAs detector arrays with a single photodiode and a simple mechanical scanning mechanism. Although the acquisition speed is lower than that of camera-based systems, the proposed architecture provides sufficient performance for laboratory beam characterization, optical alignment, and educational applications where real-time imaging is not required.

The comparison among the three scanning architectures further illustrates the trade-offs between cost, speed, and measurement capability. The rotating-detector system provides the simplest implementation and the lowest hardware cost while maintaining acceptable measurement accuracy. The single-mirror galvo architecture offers much faster one-dimensional scanning but cannot directly reconstruct a two-dimensional beam profile. The hybrid architecture provides a compromise by combining rapid galvo scanning with mechanical motion, although careful matching of the horizontal and vertical sampling resolutions is required. Finally, the dual-mirror galvo system enables the highest scanning speed and fully electronic two-dimensional scanning but requires more sophisticated optical alignment and calibration because the separation between the two mirrors introduces position-dependent beam displacement.

In addition to the demonstrated operation at 1.55 μm, the proposed beam profiler has the potential to be extended across a broad spectral range from 800 to 2600 nm by leveraging the wide spectral responsivity of the employed InGaAs photodiode. This wavelength coverage enables characterization of laser sources operating not only in the conventional telecommunications band (1.3 - 1.6 μm) but also in the emerging 2 μm and mid-shortwave infrared region [19], where applications such as eye-safe lidar, medical laser systems, environmental sensing, free-space optical communications, and thulium- and holmium-doped fiber lasers are rapidly expanding [20]. Since the measurement principle relies on mechanical beam scanning rather than wavelength-specific imaging arrays, only minor calibration adjustments are required when operating at different wavelengths. Consequently, the proposed architecture provides a versatile and cost-effective platform for beam characterization over a significantly wider wavelength range than many commercial camera-based beam profilers.

Several improvements can further enhance the performance of the proposed system. A smaller detector aperture or a longer rotating arm would improve spatial resolution, while higher-resolution motors or optical encoders could reduce mechanical positioning errors. Increasing the TIA gain and employing a higher-resolution ADC would improve the signal-to-noise ratio, allowing weaker beam wings to be measured. Future work will also investigate two-dimensional beam reconstruction and automated calibration methods for hybrid and galvo-based architectures.

6. Conclusions

This paper presents a low-cost scanning beam profiler for near-infrared laser characterization based on a rotating photodiode detector. A geometric model and detector noise model were developed to establish the spatial resolution, measurable beam size, and signal-to-noise performance of the system. Experimental measurements using a 1550 nm laser source demonstrate good agreement with both theoretical predictions and a commercial beam profiler, confirming the feasibility of the proposed approach for practical beam characterization.

Approximately 10% agreement with a commercial Thorlabs beam profiler is demonstrated over the observed operating range, with beam diameters approaching or exceeding approximately three detector aperture widths. The observed agreement is comparable in magnitude to the manufacturer-specified accuracy of commercial Thorlabs beam profilers in this wavelength range, while the proposed system costs approximately one-twentieth as much, offering a favorable performance-to-cost trade-off. Furthermore, the wavelength coverage can be extended to 2600 nm through detector substitution alone.

In addition to the experimental validation, three representative beam-profiling architectures, including the rotating-detector system, the hybrid rotating arm with a single scanning mirror, and the dual-mirror system, were analyzed and compared. Each architecture exhibits different trade-offs between hardware complexity, scanning speed, spatial resolution, and implementation cost. The proposed rotating-detector system offers the lowest-cost solution while maintaining satisfactory measurement accuracy for many laboratory applications. The comparative simulations provide quantitative guidance for selecting an appropriate beam-profiling architecture according to the required balance among cost, speed, spatial resolution, and measurement accuracy.

Overall, the presented work provides a practical framework for developing economical beam profilers for near-infrared lasers. The analytical models, experimental verification, and comparative architectural study presented in this work may serve as useful design guidelines for future low-cost laser beam characterization systems. Future work will focus on improving spatial resolution, increasing scanning speed, and extending the proposed approach to high-speed two-dimensional beam profiling.

Conflicts of Interest

The authors declare no conflicts of interest regarding the publication of this paper.

References

[1] ISO 11146-1: 2021 (2021) Lasers and Laser-Related Equipment—Test Methods for Laser Beam Widths, Divergence Angles and Beam Propagation Ratios—Part 1: Stigmatic and Simple Astigmatic Beams. International Organization for Standardization.

[2] Siegman, A.E. (1998) How to (Maybe) Measure Laser Beam Quality. Optica Publishing Group. https://doi.org/10.1364/dlai.1998.mq1

[3] Siegman, A.E. (1993) Defining, Measuring, and Optimizing Laser Beam Quality. *SPIE Proceedings*, **1868**, 2-11. https://doi.org/10.1117/12.150601

[4] Augst, S.J., Goyal, A.K., Aggarwal, R.L., Fan, T.Y. and Sanchez, A. (2003) Wavelength Beam Combining of Ytterbium Fiber Lasers. *Optics Letters*, **28**, 331-333. https://doi.org/10.1364/ol.28.000331

[5] Khalighi, M.A. and Uysal, M. (2014) Survey on Free Space Optical Communication: A Communication Theory Perspective. *IEEE Communications Surveys & Tutorials*, **16**, 2231-2258. https://doi.org/10.1109/comst.2014.2329501

[6] Ferreira, M.F.S., Castro-Camus, E., Ottaway, D.J., López-Higuera, J.M., Feng, X., Jin, W., *et al.* (2017) Roadmap on Optical Sensors. *Journal of Optics*, **19**, Article 083001. https://doi.org/10.1088/2040-8986/aa7419

[7] Meijer, J. (2004) Laser Beam Machining (LBM), State of the Art and New Opportunities. *Journal of Materials Processing Technology*, **149**, 2-17. https://doi.org/10.1016/j.jmatprotec.2004.02.003

[8] Langer, G., Hochreiner, A., Burgholzer, P. and Berer, T. (2013) A Webcam in Bayer-Mode as a Light Beam Profiler for the near Infra-Red. *Optics and Lasers in Engineering*, **51**, 571-575. https://doi.org/10.1016/j.optlaseng.2012.12.010

[9] Plass, W., Maestle, R., Wittig, K., Voss, A. and Giesen, A. (1997) High-Resolution Knife-Edge Laser Beam Profiling. *Optics Communications*, **134**, 21-24. https://doi.org/10.1016/s0030-4018(96)00527-5

[10] Chapple, P.B. (1994) Beam Waist and M2 Measurement Using a Finite Slit. *Optical Engineering*, **33**, 2461. https://doi.org/10.1117/12.169739

[11] Soto, J. (1993) Arbitrary-Intensity-Profiles Measurement of Laser Beams by a Scanning and Rotating Slit. *Applied Optics*, **32**, 7272-7276. https://doi.org/10.1364/ao.32.007272

[12] Keaveney, J. (2018) Automated Translating Beam Profiler for in Situ Laser Beam Spot-Size and Focal Position Measurements. *Review of Scientific Instruments*, **89**, Article 035114. https://doi.org/10.1063/1.5022973

[13] Alexander, S.B. (1997) Optical Communication Receiver Design. SPIE Optical Engineering Press.

[14] Moore, D.T. (1980) Gradient-index Optics: A Review. *Applied Optics*, **19**, 1035-1038. https://doi.org/10.1364/ao.19.001035

[15] Marktech Optoelectronics (2023) MTPD2601T-030 InGaAs Photodiode Datasheet. Marktech Optoelectronics, Latham, NY, USA. https://specs.marktechopto.com/pdf/products/datasheet/MTPD2601T-030.pdf

[16] Li, Y. and Katz, J. (1995) Laser Beam Scanning by Rotary Mirrors I Modeling Mirror-Scanning Devices. *Applied Optics*, **34**, 6403-6416. https://doi.org/10.1364/ao.34.006403

[17] Aylward, R.P. (1999) Advances and Technologies of Galvanometer-Based Optical Scanners. *SPIE Proceedings*, **3787**, 158-164. https://doi.org/10.1117/12.351641

[18] THORLABS (2026) BP209-IR2 Scanning-Slit Beam Profiler User Guide. Thorlabs. https://media.thorlabs.com/globalassets/items/b/bp/bp2/bp209-ir2_m/doc-104056.pdf

[19] Jackson, S.D. (2012) Towards High-Power Mid-Infrared Emission from a Fibre Laser. *Nature Photonics*, **6**, 423-431. https://doi.org/10.1038/nphoton.2012.149

[20] Heidt, A.M., Zhihong Li, and Richardson, D.J. (2014) High Power Diode-Seeded Fi-

ber Amplifiers at 2 μm—From Architectures to Applications. *IEEE Journal of Selected Topics in Quantum Electronics*, **20**, 525-536.
https://doi.org/10.1109/jstqe.2014.2312933